Journal of Energy Storage 72 (2023) 108591

Contents lists available at ScienceDirect

Journal of Energy Storage

journal homepage: www.elsevier.com/locate/est

Research Papers

Li-ion battery aging model robustness: An analysis using univariate and multivariate techniques

Enrico Marchegiani [b], Francesco Ferracuti [a], Andrea Monteriù [a], Lingkang Jin [b], Mosè Rossi [b], Gabriele Comodi [b], Lucio Ciabattoni [b,*]

[a] Marche Polytechnic University, Information Engineering Department (DII), Via Brecce Bianche 12, Ancona, 60131, Italy
[b] Marche Polytechnic University, Department of Industrial Engineering and Mathematical Sciences (DIISM), Via Brecce Bianche 12, Ancona, 60131, Italy

ARTICLE INFO

Keywords:
Battery aging modeling
Li-ion battery
Multivariate analysis
Univariate analysis
Sensitivity analysis

ABSTRACT

Batteries are highly flexible energy storages and they can be easily integrated in energy systems. However, the modeling of batteries must be coherent and robust to be effectively included in the energy systems; in particular, the aging phenomena are known to significantly impact the storage capacity, charging/discharging behaviors, and the state of charge. While data-driven lithium-ion battery models, which consider both cyclic and calendar aging, are widely reported in the scientific literature, their robustness in dealing with different data compared to trained ones has not been deeply investigated so far. In this study, a sensitivity analysis is performed using three aging models available in the scientific literature (e.g., Wang's, Baghdadi's, and Omar's ones) to investigate their performance under different operating conditions of both temperature and current. Results of both univariate and multivariate sensitivity analyses refer to a 160 A h battery, showing that all the three models are able to accurately predict the battery aging under different operating conditions, but some of these models are more sensitive to specific factors than others. Specifically, the multivariate analysis shows that Wang's model is the most robust one in the face of simultaneous changes in both temperature and current.

1. Introduction

The future energy scenario is looking at green energy sources such as renewables; however, since their energy generation is not constant, the need to store energy is becoming increasingly crucial and it will be the key point for further deploying Renewables Energy Systems (RESs) worldwide [1]. In particular, Energy Storage Systems (ESSs) will lead to an increase of connections between RESs and national grids, thus directly facing with the intermittent nature of renewables [2]. ESSs are currently being applied since they can provide the possibility of decoupling energy generation and demand, besides contributing to the grid flexibility through the supply–demand balance [3]. ESSs are classified based on the form of stored energy and their proper use is strictly dependent on the application: indeed, their technical characteristics such as energy capacity, charge/discharge dynamics, self-discharge rate, energy–power ratio, and life cycles have to be carefully considered for choosing the most suitable technology for a specific application [4].

In the energy sector, the most used storage technology in large-scale application is the Battery Energy Storage System (BESS) due to the high flexibility and regulation capacity [5]. Several studies investigated on the effect of the BESS integration in national grids, highlighting the advantages in terms of both costs and load management [6,7]. However, the future application of BESSs is not only focused on large-scale applications, but also in small-scale ones (e.g., residential building, offices, energy intensive industries, and Electric Vehicles (EVs) charging stations). In this regard, the authors of [8,9] analyzed Photovoltaics (PV)-BESS systems used in commercial, residential, industrial, and healthcare contexts by developing and studying several scenarios to improve their operation. BESSs are mainly Li-Ion based, which consist of a highly modular technology that can be applied at different scales as discussed by [10].

BESSs are highly versatile and they need coherent and reliable models, which are based on proper scenarios, to be used as input for the planning phase. This approach must include aging models since the degradation aspect influences directly the overall storable energy, charging/discharging behaviors, and its State Of Charge (SOC). The aging phenomena become even more important when Li-Ion batteries are studied for second life purposes in the power sector after they have reached the End Of Life (EOL) in the automotive one [11], which consists of a residual energy equal to 80% of the rated one [12].

* Corresponding author.
E-mail address: l.ciabattoni@staff.univpm.it (L. Ciabattoni).

https://doi.org/10.1016/j.est.2023.108591
Received 17 January 2023; Received in revised form 30 June 2023; Accepted 31 July 2023
Available online 18 August 2023

Nomenclature

BESS	Battery Energy Storage System
BMS	Battery Management System
C/LFP	graphite anode/lithium iron phosphate cathode
C_0	Nominal capacity
C_{res}	Residual capacity
Crate	Current rate
DOD	Depth Of Discharge
ELM	extreme learning machine
EOL	End Of Life
ESS	Energy Storage System
EV	Electric Vehicle
MAE	Mean Absolute Error
MAPE	Mean Average Percentage Error
PSO	Particle Swarm Optimisation
PV	Photovoltaics
R_0	Internal resistance
RES	Renewables Energy System
RMSE	Root Mean Square Error
RUL	Remaining Useful Life
SOC	State Of Charge
SOE	State Of Energy
SOH	State Of Health
T	Temperature
t	Time
XGBoost	eXtreme Gradient Boosting

Different studies in the scientific literature aimed at describing the aging phenomena from a microscopical point of view, involving the electrochemical mechanisms due to the use of Li-ions, as well as active resources at both anode and cathode materials [13–15]. Along the same line, a particular attention has been devoted to the aging problem and its effects according to the principal macroscopic quantities such as temperature, charge/discharge current, Depth Of Discharge (DOD), and SOC that are easily obtainable in real contexts. These studies presented aging models that describe the degradation dynamics, as well as both use and implementation of BESSs. The authors of [16] proposed a numerical model for the State Of Health (SOH) estimation of grid-connected BESSs based on the efficiency index that is estimated by two test protocols built around standard equipment and charge/discharge tests, respectively. The authors of [17] built on a SimPowerSystems block that is used to model the charge and the discharge dynamics of the battery, as well as simulate the aging effects due to cycling. The model is validated experimentally with four types of batteries. A similar model developed in SimPowerSystem is proposed in [18] where the aging is estimated in terms of number of charge–discharge cycles that the cell has done during its life. The authors of [19] integrated the effects of both temperature and SOH variations in the battery model. The aging model, which is based on the battery State Of Energy (SOE) [20], depends on the battery temperature and voltage or SOC. Reduction of the energy storage capability of the battery is considered by an aging model consisting of both calendar and cycle aging models. The authors of [21] developed an adaptive partial differential equation observer for estimating the SOH of the battery, while the behavior of Li-Ion batteries has been addressed in [22] by focusing on the graphite anode/lithium iron phosphate cathode (C/LFP) batteries during the calendar life at different storage conditions. An overview of the available methods and algorithms related to the on-board capacity estimation of Li-Ion batteries is proposed in [23]. The maximum energy storage capability estimation acts as an indicator for the SOH of a battery and the estimation of the remaining useful life. Battery SOH monitoring methods are reviewed in detail in [24]. The authors of [25] presented an overview of the different proposed battery, thermal, and aging models classified in three categories: mathematical, physical, and circuit models. The authors of [26] investigated on the degradation of the internal resistance of a Li-Ion battery based on extended laboratory calendar aging tests. Starting from the model described by [27], a generic one used to evaluate the cycling fade at each time step is proposed in [28] for being applied then in the automotive sector. Li et al. [29] introduced the application of a rain-flow algorithm for cycle counting and a battery aging index based on both DOD and Crate. Omar et al. [30] proposed univariate models and a least-square fitting method for the cycle aging estimation. Wang et al. [27] developed a life cycle model for C/LFP batteries. The model has been developed based on experimental results, whereby the proposed battery has been cycled at different operating conditions in terms of temperatures, current rates, and DODs. Zabala et al. [31] proposed a combined calendar and cycle aging that has been investigated with dynamic and realistic complex operating profiles. Baghdadi et al. [32] studied the effect of calendar and power cycling aging on two different battery technologies under different operating conditions, proposing a battery aging rate index that depends on the current, temperature, and battery SOC.

In the following works, data-driven approaches are proposed to estimate the SOH of a battery. The authors of [33] conducted a detailed review on the current state of data-driven techniques, specifically focusing on machine learning methods for predicting both SOC and SOH of batteries. They analyzed various machine learning techniques' performance by comparing them with equivalent circuit and physics-based models. Despite the vast amount of studies, there is still a major challenge in estimating the SOH due to modeling accuracy over time, in situ calculations, and high-throughput data generation. The authors of [34] used the Gaussian process regression method to build a data-driven estimator with a two–stage feature extraction and feature optimization approach, which has been validated using two different datasets: Oxford [35] and Maryland [36]. They evaluated the estimation performance using mean absolute error, the root-mean-squared error, and the maximum error metrics which were resulted equal to 16.36%, 32.43%, and 45.46%, respectively. The authors of [37] investigated on the nonlinear frequency response analysis tool for data-driven SOH identification of Li-Ion batteries. The authors of [38] proposed a joint model-based and extreme learning machine(ELM)-oriented framework for estimating the SOH of batteries. The authors of [39] discussed about a joint estimator using a double extended Kalman filter for estimating the SOH of batteries as well. A similar approach based on the Kalman filter and support vector regression is described in [40]. In [41], the main features are extracted from voltage data and they are scored based on prognostic metrics to select diagnostic features that can conveniently identify the degradation of a battery. Afterwards, an ensemble learning model has been developed to capture the correlation of diagnostic features and the SOH of a battery. The authors of [42] presented a novel ensemble learning framework to estimate the SOH of a battery and a self-adaptive differential evolution algorithm to effectively integrate the weak learners, thus avoiding the trial and error procedure to choose the trial vector generation strategy and the related parameters in the traditional differential evolution. The authors of [43] extracted several features that describe the aging processes of the batteries to build up an eXtreme Gradient Boosting (XGBoost) model for estimating the SOH of batteries. Then, the estimation value has been corrected by the Markov's chain. A state-of-the-art of data-driven approaches related to the estimation of the SOH of batteries is reported in [44]. Finally, a battery degradation model has been investigated using an electro-chemical-thermal model built up with Comsol Multiphysic [45]. Yang et al. [46] conducted a comprehensive analysis by collecting characteristic parameters from both cell and pack levels, proposing a monitoring, diagnostics, and prognostics procedure. Tian

Table 1
Aging models: the current state-of-the-art.

Reference	Calendar aging	Cycle aging	Completeness	Review	Not validated	Model-based
Tremblay et al. [17]		√				√
Huria et al. [18]		√				√
Barrera et al. [19]		√				√
Guenther et al. [20]	√	√	√			√
Moura et al. [21]		√			√	√
Omar et al. [22]	√					√
Farmann et al. [23]				√		√
Berecibar et al. [24]				√		√
Barcellona et al. [25]				√		√
Stroe et al. [26]	√		√			√
Yuksel et al. [28]		√	√		√	√
Li et al. [29]		√				√
Wang et al. [27]		√	√			√
Omar et al. [30]		√	√			√
Baghdadi et al. [32]	√	√	√			√
Zabala et al. [31]	√	√	√			√
Ragone et al. [45]		√				√
Rancilio et al. [16]		√				
Harting et al. [37]		√				
Pan et al. [38]		√				
Fang et al. [39]		√				
Khaleghi et al. [41]		√				
Meng et al. [42]		√				
Song et al. [43]		√				
Vidal et al. [44]		√				
Andre at al. [40]		√				
Ng et al. [33]				√		
Huang et al. [34]		√	√		√	
Yang et al. [46]				√		
Tian et al. [47]				√		

et al. [47] divided several SOH estimation methods into five groups: (i) equivalent-circuit-model-based (ii) aging mechanism-based, (iii) electrochemical impedance spectroscopy-based, (iv) empirical degradation model-based, and (v) probabilistic-based. Furthermore, these methods can be also divided in data-driven techniques (e.g., artificial neural network, support vector machine, and relevance vector machine).

Table 1 lists the works previously described, showing the points addressed by each study. In particular, *calendar aging* and *cycle aging* refer to works that proposed calendar or cycle aging models. *Completeness* defines whether the model involves most of the macroscopic variables that mainly affect the degradation of BESSs (e.g., SOC, DOD, Crate, and temperature). *Review* refers to works that present a literature review of the battery aging. *Not validate* refers to works where the battery aging model has not been validated with real experiments. Finally, *Model-based* refers to works whose proposed model is either a first principle or a mathematical equation; otherwise, the model has been built up using a data-driven approach.

According to the literature review, both development and training of a feasible aging model for being used in real applications is still a challenging task. The training phase should produce a model that is able to represent appropriately the degradation behavior of a specific BESS, but the model has to be robust when different input values are used in the training process. Regarding the real cases, a solution that is not able to generalize over different data, even if it varies hugely when subjected to small variations, must be avoided since the operating conditions of BESSs cannot be controlled and can present different profiles. Acquired dataset are usually referred to one or more specific operating conditions that do not cover a wide range of intensities, type of usage, weather conditions, and other specific parameters.

Despite an extensive review of the scientific literature on BESS' aging models, to the authors' knowledge, none of the articles investigated so far incorporate a sensitivity analysis to assess the models' response to input variations post-training. Indeed, this is a crucial aspect that still remains unexplored, highlighting the need for a further insight to fully understand the robustness and the reliability of these models in practical scenarios. Hence, this work presents a sensitivity analysis on how a model deals with an unexpected variation from the input variables compared to the training dataset. Three aging models are chosen due to their reasonable performance on describing the aging behavior in terms of model completeness, ease of training, and frequent use in the scientific literature. Results computed by these models have been obtained by considering a 160 A h BESS and then compared and discussed once the univariate sensitivity analysis (e.g., temperature or current values are changed by keeping the other fixed) and multivariate sensitivity analysis (e.g., both temperature and current are varied) have been performed. It is worth noting that the values used for the training process are different from those used for the testing process.

The paper is structured as follows: Section 2 deals with aging characterization, the methodology, and the models involved in this analysis. Section 3 presents the results obtained, and Section 4 reports the conclusions of this work.

2. Methods

This section describes the aging phenomena of Li-ion batteries, delving into the underlying causes and involved mechanisms. Section 2.1 provides an in-depth explanation of the performed sensitivity analysis procedure, including a technical explanation of the used statistical methods such as univariate and multivariate analyses. Finally, a comprehensive summary of the analyzed models is presented.

2.1. Li-Ion battery aging characterization

The microscopic aging mechanism is strictly related to the conditions at which the battery is exposed, and it occurs when the storage is whether maintained at rest or cycled. These conditions determine the aging type that affects the storage, namely known as calendar or cycle aging. Both aging modes coexist during the battery life; however, the study of the combined effect is not trivial and the scientific community mainly deals with them separately as reported in Table 1. The calendar aging comprises all the mechanisms that occur when the battery is at rest, stocked at fixed conditions; thus, it is directly dependent on the storage temperature and the SOC level of the battery. Conversely, the cycle aging is characterized by the cycling operating condition

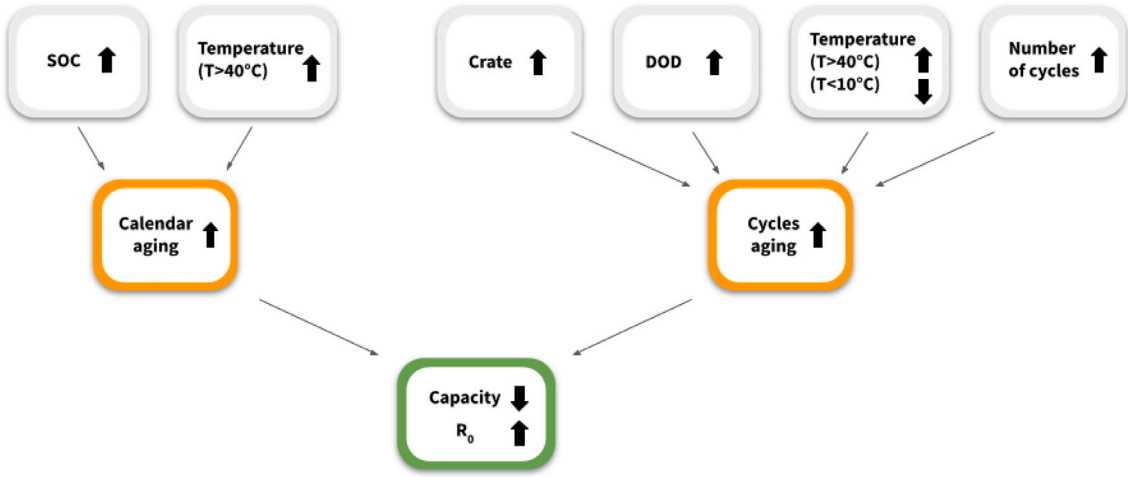

Fig. 1. Relation between calendar and cycle aging: as a result, the capacity drops and the resistance increases.

of the batteries, whose main factors are temperature (e.g., ambient, pack or cell), DOD, charge or discharge current (Crate) and number of cycles [11]. Fig. 1 shows the relations between the two different aging modes as well as the main parameters that affect each mode.

As reported in Fig. 1, both aging modes, even with different causes, have the same effects; indeed, they increase the internal resistance of the battery that worsen its power performance, but also decreases the storage capacity [48]. The internal resistance, which is usually indicated as R_0, determines the energy dissipated as heat due to the Joule effect: it is worth noting that R_0 cannot be measured directly, but its rated value is usually reported in the data-sheets. R_0 differs significantly from the resistance that can be estimated from the electrical model, and it depends on the amount of current injected into the battery.

In addition to the aging phenomena, R_0 generally relies on both temperature and SOC level. The resistance drops instantaneously when the temperature raises and vice versa [49]. The operation of the batteries at high temperatures is inconvenient since it leads to a considerable degradation of the battery due to the Joule effect. However, the effect of the SOC level on R_0 of the Li-Ion batteries is considered marginal compared to its variation generated by both aging modes and operating temperature [50].

The maximum capacity of a battery C and its residual capacity C_{res} indicate the maximum amount of charge that the system is able to store and release. They cannot be measured directly and so they must be estimated by the Battery Management System (BMS) that computes the amount of energy that is extracted or introduced into the system itself. The residual capacity estimation is a challenging task and may be updated more precisely with deeper operating cycles, whereas it presents several issues in case of brief charge and discharge cycles. Such a quantity depends on both aging and temperature similarly to R_0 [51]. Since there is a strong relationship between the residual capacity and the aging of the BESS, the residual capacity is considered the main parameter to define the SOH of a battery. Typically, the SOH of a battery is defined as the ratio between the residual C_{res} and the rated capacity C_0 according to Eq. (1):

$$SOH(t) = \frac{C_{res}(t)}{C_0} \tag{1}$$

Moreover, R_0 plays a key role in defining the SOH, albeit with less prominence in the scientific literature. Thus, the specific formula that relates R_0 with the SOH has not been provided in this work since it is out of the scope of the current study. The SOH value is the determining factor to define the EOL, and it is specifically tailored for each application according to the minimum operative conditions required by the storage system. For instance, the EOL for automotive applications is usually set equal to 80% since the residual capacity reflects the vehicle range. A similar metric to EOL is the remaining useful life (RUL) that defines the residual operating life of a BESS, which is usually expressed in number of cycles.

Table 2
Operating conditions of simulated data through the univariate analysis.

Temperature	20 °C	25 °C	30 °C	35 °C	
Current	0.1 C	0.25 C	0.5 C	0.75 C	1 C

2.2. Sensitivity analysis

In this work, a sensitivity analysis, which aims to evaluate the robustness of models and how these deal with an unexpected variation in the input variables compared to the training dataset, is conducted. This analysis allows to identify which parameters have the greatest impact on model predictions and determine the range of values over which a specific model is most accurate. This study considers the variation of both temperature and current since they represent the principal cycling factors that impact on the battery life [52].

Univariate and multivariate analyses are performed to study how the variation of a single quantity, or both quantities simultaneously, affects the model response. Each aging model is described by parametric equation as defined in Section 2.3: the analysis comprises firstly a training phase to compute model parameters that are then tested on another dataset. Simulated data are obtained with an algorithm based on a least-squares support-vector machines model, which has been trained using experimental data obtained by [30]. As a result, a simulated dataset of a 160 A h BESS is used in these analyses.

Regarding the univariate analysis, data are obtained by changing the temperature and keeping fixed the current and vice versa. Temperature and current values for the univariate analysis are changed as shown in Table 2.

A residual capacity curve is generated per each value as shown in Figs. 2 and 3. The models are trained considering current values of 0.1 C and 1 C and, temperature values of 20 °C and 35 °C; then, each model previously trained is tested to the excluded values, namely 0.25 C, 0.5 C, and 0.75 C concerning the current and 25 °C and 30 °C regarding the temperature.

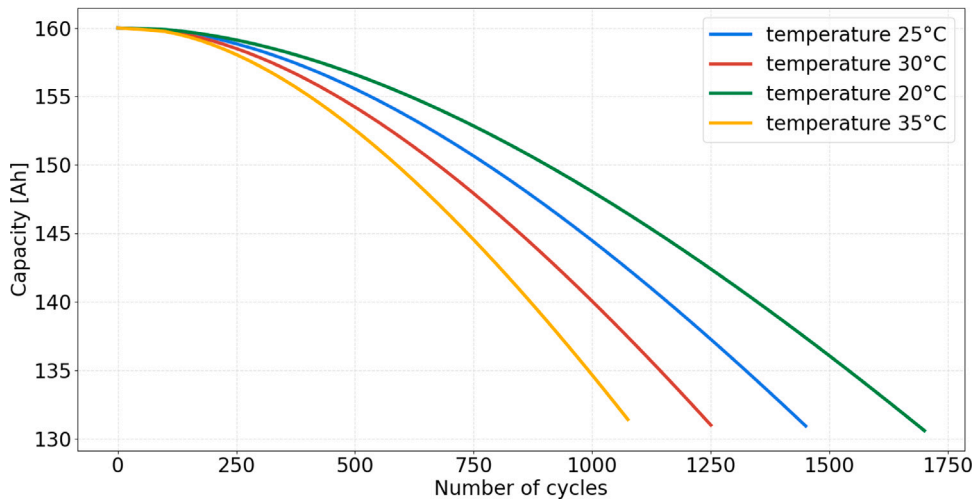

Fig. 2. Simulated dataset used for the temperature sensitivity analysis: the residual capacity of the battery is plotted as a function of the number of cycles. Temperature values range from 20 °C to 35 °C.

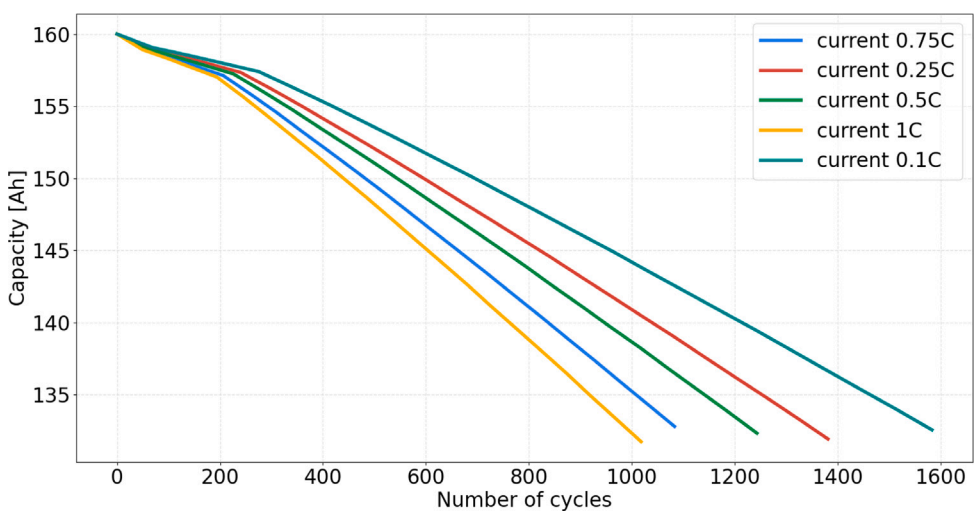

Fig. 3. Simulated dataset used for the current sensitivity analysis: the residual capacity of the battery is plotted as a function of the number of cycles. Current values range from 0.1 C to 1 C.

Conversely, the dataset used for the multivariate analysis is composed by degradation curves that are generated using different temperature and current as reported in Fig. 4. The value pairs reported in Table 3 are the operating conditions simulated to resemble the aging phenomena for the multivariate analysis.

It is worth noting that only the pairs (0.1 C, 20 °C) and (1C, 35 °C) have been used for the training process, while the remaining ones have been employed for the model testing.

The values used for the testing phase are those that have not been used in the training process of both univariate and multivariate analyses. The other parameters that affect an aging degradation are kept fixed as reported in Table 4.

The Particle Swarm Optimisation (PSO) algorithm [53] is used to get the optimum model parameters due to its effectiveness to deal with non linear functions.

Table 3
Variation in operating conditions of simulated data for the multivariate analysis. Temperature and current are simultaneously changed.

Temperature	Current
20 °C	0.1 C
24 °C	0.25 C
27.5 °C	0.5 C
31 °C	0.75 C
35 °C	1 C

2.3. Selected aging models

In this work, three models described in the scientific literature have been selected to assess the aging phenomena of the simulated 160 A h BESS [27,30,32]. These models have been chosen due to their completeness in terms of inclusion of the principal macroscopic quantities affecting the aging phenomena (e.g., temperature, charge/discharge current, DOD, SOC, easiness of training, and frequent employment in the scientific literature). The authors of [30] used four mathematical

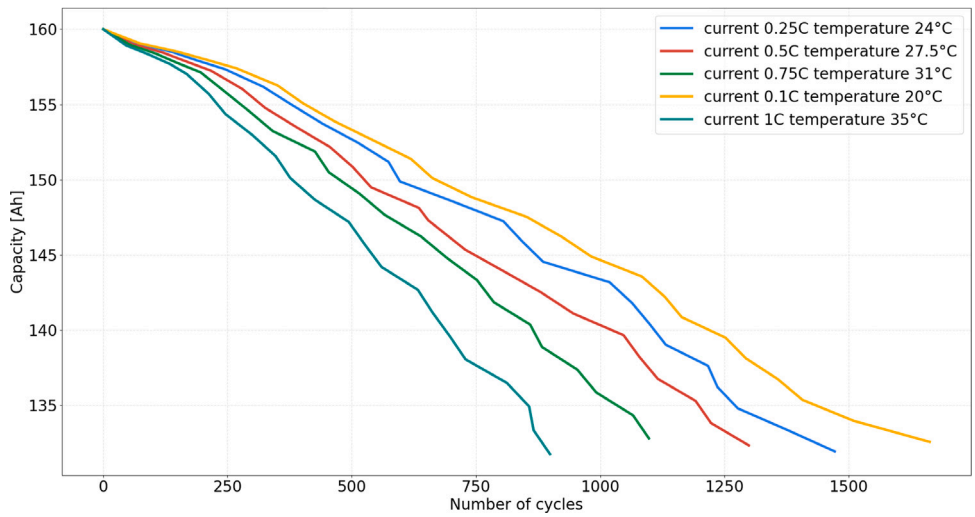

Fig. 4. Dataset used for the multivariate sensitivity analysis: the residual capacity of the battery is plotted as a function of the number of cycles. Temperature values range from 20 °C to 35 °C, while the current ones between 0.1 C and 1 C.

Table 4
Other parameters used in the testing process.

Fixed input	Values	Notes
DOD	85%	Depth Of Discharge in each cycle
SOC average	50%	Average SOC level in each cycle
Crate	0.1 C	Current fixed in the univariate temperature analysis
T	20 °C	Temperature fixed in the univariate current analysis

equations to describe the data acquisition separately based on the variation of the principal quantities affecting the aging phenomena. Since the input variables are treated individually, these models can be easily trained. Wang et al. [27] used an exponential model that is widely employed when dealing with cumulative degradation dynamics due to its robustness and easier identification procedure of the parameters [54]. The authors of [32] implemented both calendar and cycle aging using only one model, thus improving its application when dealing with several conditions. The selected models are further discussed in Section 2. In the following Subsections, the three aging models selected for the sensitivity analyses are described in detail.

2.3.1. Baghdadi [32]

The proposed model is the most comprehensive among the selected ones, but it is the more complex due to a high potential risk of over fitting. Indeed, it returns the maximum capacity available at a defined time and considers both cycle and calendar aging phenomena. It is based on the computation of two parameters, namely k_{cyc} and k_{cal}, that are related to cycle and calendar aging, respectively, thus leading to a possible application in different real contexts simultaneously. The model approach aims at reproducing a chemical rate based on the Dakin's degradation.

$$k_{cal}(T, SOC) = \exp(k_1 \frac{SOC}{R}) \cdot \exp(\frac{k_2}{R}) \cdot \exp(-\frac{k_3}{RT}) \tag{2}$$

$$a(T) = \exp(\frac{k_4}{RT} + k_5) \tag{3}$$

$$k_{cyc} = \exp(a(T) \cdot \frac{I}{I_0}) \tag{4}$$

$$k_{tot} = k_{cal} \cdot k_{cyc} \tag{5}$$

$$C(t) = C_0 \exp(-k_{tot} t^{k_6}) \tag{6}$$

Application: energy and power intensive contexts.

Input: SOC [%], temperature [K], time [d], and current [A].

Parameters: k_1, k_2 [J mol^{-1} K^{-1}], k_3, k_4 [J mol^{-1}], k_5, k_6 dimensionless

Coefficients: I_0, reference current A; C_0, rated capacity expressed in A h; R, universal gas constant expressed in J mol^{-1} K^{-1}.

Outputs: $C(t)$ that is the capacity at a specific time expressed in A h.

Storage size: validated with two storage at 5.3 A h and 4.2 V and 7 A h and 4 V, scalable to other sizes.

Pros: both calendar and cycle aging are considered.

Cons: the model validation proposed is performed by keeping constant both SOC and temperature; furthermore, the analysis is focused on a single Li-ion cell, thus ignoring the internal resistance variation.

Note: the calendar contribution computation is simplified. Differently from this model that computes the calendar factor as the average of k_{cal} with respect to the SOC interval, the calendar contribution is evaluated using the average SOC of charge and discharge cycles.

2.3.2. Wang [27]

This model evaluates the capacity loss as a percentage of the current used and injected in the electric storage. It is worth noting that the exponential modeling is already widely used in the scientific literature.

$$Q_{loss} = k_1 \cdot \exp\left(\frac{k_3 + 370 \cdot C_{rate}}{RT}\right) \cdot (A\ h)^{k_2} \tag{7}$$

Application: energy- and power-intensive contexts.

Inputs: temperature [K], total amount of capacity supplied and extracted to and from the battery [Ah], Crate.

Parameters: k_1, k_2 dimensionless, k_3 [J mol^{-1}].

Output: Q_{loss} [%] that is the capacity loss in percentage due to the aging phenomenon.

Storage size: validated with 2.2 Ah with 3.6 V, scalable to other sizes of storage.

Pro: computational efficiency and robustness due to the single exponential equation. Inputs data always noted.

Cons: a single exponential model does not adequately describe the high variation of the quantities. Different training are needed based on the operating conditions.

Note: k_3 is an additional parameter that improves the model performance instead of using a constant value as in the original study.

2.3.3. Omar [30]

These models allow to define the degradation of a battery in terms of life cycles (e.g., RUL to achieve the 80% of the residual capacity due to the effect of the cycle aging). Each model is univariate, meaning that it evaluates the aging effect according to the variation of a single input,

while the remaining ones are kept fixed. Since the interest of this study is restricted to temperature and current analyses, only the models that include them are here reported.

$$CL(T) = k_1 T^2 + k_2 T + k_3 \tag{8}$$

$$CL(I_d) = k_1 \exp(k_2 I_d) + k_3 \exp(k_4 I_d) \tag{9}$$

Application field: energy- and power-intensive contexts.

Inputs: temperature [K] and Crate (I_d).

Parameters: k_1 [K^{-2}], k_2 [K^{-1}], $k_i, i = 3, \ldots, 5$ dimensionless.

Outputs: Cycle life or RUL of the battery expressed in number of cycles.

Storage size: 2.3 Ah with 3.3 V. It is scalable to other dimensions.

Pros: it allows to study multiple parameters regarding the aging. It has been also experimentally tested and validated.

Cons: the variables that are not evaluated through equations are considered as constant parameters. Since each model equation evaluates the aging based on the variation of a single input quantity, they are not suitable for performing multivariate analysis. Consequently, Omar's model will not be included in the multivariate analysis study.

Note: the polynomial Eq. (8) is reduced down to one degree with respect to the model proposed in the literature. The simplification is introduced to avoid over fitting and simplify the training phase since the coefficient relative to the third degree term is evaluated to be close to zero. Since these models estimate the number of cycles executed to reach a specific capacity threshold, many set of parameters are computed, each for a different residual capacity value, so that the capacity degradation curve can be modeled. Moreover, k_1 is forced to be lower than zero according to data reported in [30] regarding the temperature modeling.

The main metrics used to compare the effectiveness of the used models is the Mean Average Percentage Error (MAPE) as described in Eq. (10). This parameter provides a coherent comparison between the models of [27,32] because the outputs are the same (e.g., capacity), while it represents an error indication in all the models of [30] whose outputs are expressed in terms of number of cycles at a different scale.

$$MAPE = \frac{100\%}{n} \sum_{t=1}^{n} \left| \frac{y_t - \hat{y}_t}{y_t} \right| \tag{10}$$

Moreover, for the sake of completeness, the maximum error, the Mean Absolute Error (MAE), and the Root Mean Square Error (RMSE) are reported for each model as described in Eqs. (11) and (12).

$$MAE = \frac{1}{n} \sum_{t=1}^{n} \left| y_t - \hat{y}_t \right| \tag{11}$$

$$RMSE = \sqrt{\frac{1}{n} \sum_{t=1}^{n} \left(y_t - \hat{y}_t \right)^2} \tag{12}$$

3. Results and comments

In this work, the results of the aging models on a simulated 160 A h BESS are analyzed. Different data of temperature and current are employed in the training and evaluation phase to define which model provides a more reliable and robust characterization. In particular, both temperature and current are varied either singularly or simultaneously while keeping the other quantities unchanged. Regarding the temperature analysis, 20 °C and 35 °C values are arbitrarily used for the training process, while 25 °C and 30 °C are used for the testing one. Regarding the current analysis, the models are arbitrarily trained using values of 0.1 C and 1 C, and they are tested with values of 0.25 C, 0.5 C, and 0.75 C. In the multivariate analysis, the models are trained using the following pairs (0.1 C, 20 °C) and (1 C, 35 °C), while (0.25 C, 24 °C), (0.5 C, 27.5 °C) and (0.75 C, 31 °C) are employed in the testing process. Results obtained by both univariate and multivariate analyses are presented separately in addition to the corresponding parameters computed and the MAPE values.

Table 5
Baghdadi's model parameters related to the temperature sensitivity analysis.

k1	k2	k3	k4	k5	k6
4565.029	−2298.808	4999.728	1.331	−1874.153	−2389.017

Table 6
Wang's model parameters related to the temperature sensitivity analysis.

k1	k2	k3
6.362×10^{-6}	1.228	−799.922

Table 7
Omar's model parameters describing temperature effect on aging.

C_{res}[%]	k1	k2	k3
100	−0.261	14.332	−82.402
99.375	−0.595	26.041	17.054
98.125	−0.981	40.631	79.844
96.875	−1.259	55.916	−14.692
93.75	−1.978	88.767	−84.313
91.25	−2.345	102.314	−8.235
86.875	−3.060	134.971	−75.395

3.1. Univariate temperature

The parameters trained for analyzing the temperature sensitivity are reported in Tables 5, 6, and 7. Each model is characterized by a different number of parameters according to the mathematical equations described in Section 2.3. In [32], the six parameters that characterize the equations assume very large numbers, thus highlighting the risk of being sensible to variations since several combined exponential functions are embedded in the model.

The three Wang's parameters [27] are computed and a very low $k1$ value (modulus) is obtained.

As described in Section 2.3.3, Omar's equations [30] model the degradation of a battery in terms of the number of cycles required to reach a determined residual capacity. Since the equation describing the temperature effect on the battery aging is defined by three parameters, seven sets of three parameters are computed, one for each value of the residual capacity threshold listed in the first column of Table 7. The model is trained on seven levels of the residual capacity, returning the same number of set of parameters that are used to compute the error obtained by the simulated curves in terms of number of cycles.

Then, the proposed model is tested by simulating the capacity curves related to 25 °C and 30 °C and compared to the ones of the Baghdadi's model using the same temperature values previously mentioned. Fig. 5 shows that the Baghdadi's model follows the decreasing trend of the simulated curves, reaching a maximum error of 8.04 A h, a MAE of 1.82 A h, and a RMSE of 2.52 A h. The match of the 30 °C curves is decent between 0 and 600 number of cycles, while the difference is more noticeable afterwards, where the model trend lead the simulation to diverge more markedly from the data. A similar trend is obtained by the 25 °C curves, even though the difference between the simulated and the Baghdadi's model is more remarkable between 0 and 1000 number of cycles.

Similar results are obtained with the Wang's model, even though a slight increase of the error is obtained by reaching a maximum error of 9.1 A h, a MAE of 2.09 A h, and a RMSE of 2.9 A h. Fig. 6 shows the Wang's model tested at 25 °C and 30 °C with red and blue lines: also in this case, the behavior described by both green and yellow curves is similar to the Wang's curves. Finally, differently from Baghdadi and Wang's models, the number of cycles required to reach a particular residual capacity related to the respective set of parameters are computed using the Omar's model. Fig. 7 shows the results at 25 °C and 30 °C, which slightly overestimates simulated data, reaching a

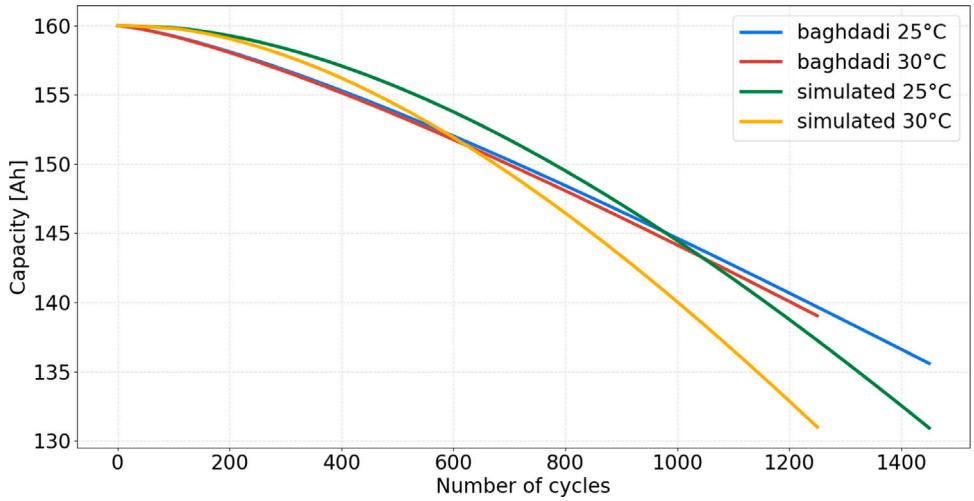

Fig. 5. Baghdadi's model tested at 25 °C and 30 °C.

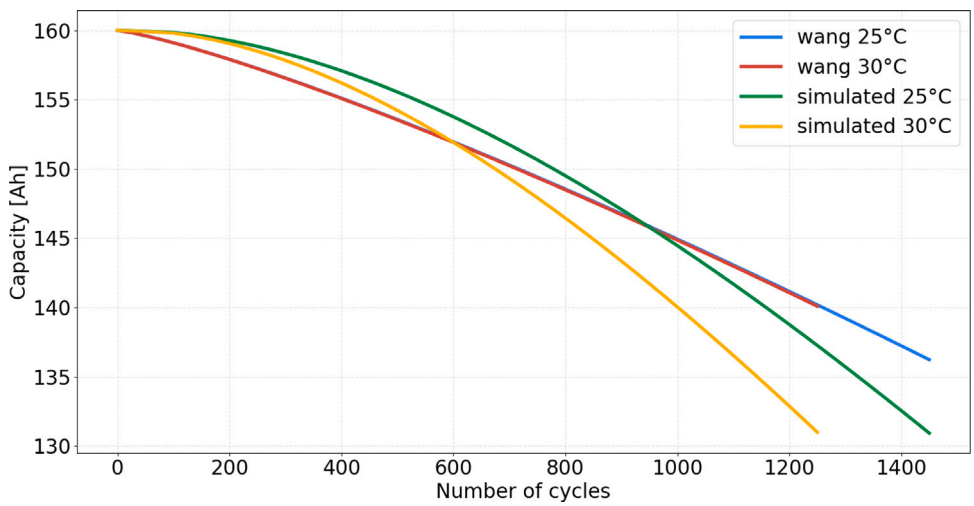

Fig. 6. Wang's model tested at 25 °C and 30 °C.

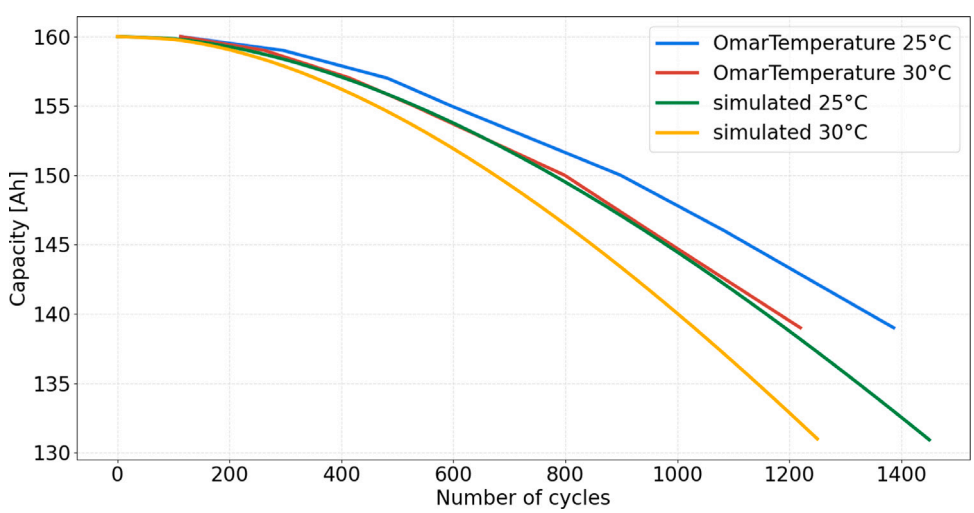

Fig. 7. Omar's model depending on temperature tested at 25 °C and 30 °C.

Table 8
MAPE computed in the temperature sensitivity analysis.

Temperature	Wang	Baghdadi	Omar
25 °C	1.19%	1.05%	14%
30 °C	1.79%	1.54%	14%

Table 9
Baghdadi's model parameters related to the current sensitivity analysis.

k1	k2	k3	k4	k5	k6
2661.486	−1361.219	−318.699	1.319	−1096.049	1.713

Table 10
Wang's model parameters related to the current sensitivity analysis.

k1	k2	k3
9.81×10^{-6}	1.25	−635.86

maximum error of 195 cycles, a MAE of 84 cycles, and a RMSE of 102 cycles for the seven modeled values.

The MAPE that was computed to compare the models performances is reported in Table 8. Among the studied models, the most robust one when dealing with temperature variations is the Baghdadi's model for both 25 °C and 30 °C. A slightly worse performance is obtained by using the Omar's model, particularly at 30 °C curve. Conversely to the other models, the Omar's one is not a viable solution as it solely considers a single quantity and requires a more complex parameter computation, making it unfeasible in practical applications. Although both Baghdadi and Wang's models cannot significantly discriminate the aging evaluation among the two values of the temperature, the Baghdadi's model is slightly more robust and represents the best choice when considering the temperature variations. However, experimental data reported by Omar et al. [30] indicate that 20 °C is the optimal temperature condition that ensures a greater RUL, whereas a decrease of the life cycles is expected with temperature lower and greater than 20 °C. Conversely to the Omar's model that describes each residual capacity point at different temperatures with a concave downward parabola, Baghdadi and Wang's models are not able to reproduce that behavior, unless a training curve with temperatures lower than 20 °C is used. Therefore, further models should be investigated as possible future development.

3.2. Univariate current

According to the mathematical models described in Section 2.3, the parameters trained for analyzing the current sensitivity are reported in Tables 9, 10, and 11. Similarly to the univariate analysis of the temperature variation, the Baghdadi's model parameters [32] assume very large numbers, thus highlighting the risk of being sensible to variations since the double exponential functions are embedded in the model.

The three Wang's parameters [27] return a very low $k1$ parameter value (modulus).

Similarly to the temperature analysis, a set of four parameters is computed for the Omar's model [30] for each value of capacity thresholds, which are reported in the first column of Table 11. The model is trained on sixteen levels of residual capacity and it returns the same number of parameters set that are used to compute the error from the simulated curves in terms of number of cycles.

All the models are tested with capacity curves related to 0.25 C, 0.5 C, and 0.75 C. Fig. 8 shows that the Baghdadi's model [32], which was tested using current values of 0.25 C, 0.5 C, and 0.75 C (red, blue, and green lines), overestimates the simulated data (orange, yellow, and aqua green curves) reaching a maximum error of 14.87 A h, a MAE of 6.15 A h, and a RMSE of 7.54 A h.

Table 11
Omar's model parameters related to the current sensitivity analysis: each row is related to the residual capacity threshold of the first column.

C_{res}[%]	k1	k2	k3	k4
100	13.69	−989.066	−20.44	−993.074
99.375	274.123	−675.799	84.245	−0.770
98.75	116	4.257×10^{-17}	667.176	−479.812
98.125	155	2.606×10^{-9}	219.112	−202.168
97.5	194	-1.449×10^{-14}	−229.219	−321.364
96.25	275.588	−0.168	231.643	−686.973
95.625	314.666	−0.149	160.136	−391.729
93.75	392.599	−0.118	−296.494	−498.801
93.125	430.445	−0.104	−464.388	−538.636
91.25	508.53	−0.089	197.177	−987.357
90	590.251	−0.158	181.206	−302.273
88.125	83.219	−109.698	668.287	−0.14
87.5	707.251	−0.132	173.989	−699.821
86.25	745.093	−0.123	−273.609	−385.423
84.375	823.162	−0.112	−270.926	−775.372
83.125	−302.86	−274.405	904.916	−0.155

Table 12
MAPE computed in the current sensitivity analysis.

Crate	Wang	Baghdadi	Omar
0.25 C	0.85%	4.83%	16.53%
0.5 C	0.96%	4.84%	13.46%
0.75 C	1.26%	3.09%	10.18%

Table 13
Baghdadi's model parameters related to the multivariate sensitivity analysis.

k1	k2	k3	k4	k5	k6
1613.759	−839.279	1009.548	1.296	−1741.983	2.091

Fig. 9 shows that the Wang's model performance [27] when tested at 0.25 C, 0.5 C and 0.75 C follows the simulated data; however, it presents a strong linear behavior that highlights a moderate robustness with respect to the variation of Crate. Numerical results report a maximum error of 5.30 A h, a MAE of 1.45 A h, and a RMSE of 1.85 A h.

Along with the Wang's model results, the Omar's model [30] significantly represents simulated data, underlying its robustness as well.

Fig. 10 shows the Omar's model tested at 0.25 C, 0.5 C, and 0.75 C, representing the sixteen residual capacity values over the number of cycles estimated by the model: it reaches a maximum error of 127 cycles, a MAE of 37 cycles, and a RMSE of 50 cycles. The MAPE that was computed for the current sensitivity analysis to compare all the models performances is reported in Table 12, where the most robust one is the Wang's model for all Crate values. The worst performance has been obtained by the Omar's model, particularly at 0.25 C. Moreover, since the Omar's model does not consider any other quantities and involves a more complex training phase obtaining a set of parameter for each capacity value, it does not represent a feasible solution compared to the others. The Baghdadi's model does not perform as the Wang's model does, achieving a MAE of 5.72 A h; thus, the Wang's model is the most robust and represent the best choice when considering current variations.

3.3. Multivariate analysis

According to the mathematical models described in Section 2.3, the parameters trained for the multivariate sensitivity are reported in Tables 13 and 14. Baghdadi's model parameters [32] assume very large numbers, thus highlighting the risk of being sensible to variations since the double exponential functions are embedded in the model.

The three Wang's parameters [27] return a huge $k1$ parameter value (modulus).

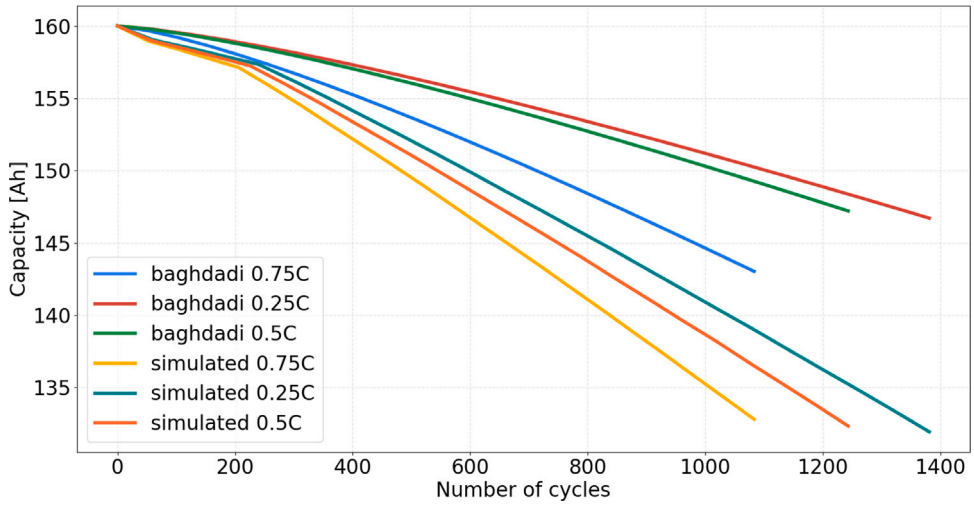

Fig. 8. Baghdadi's model tested at 0.25 C, 0.5 C, and 0.75 C.

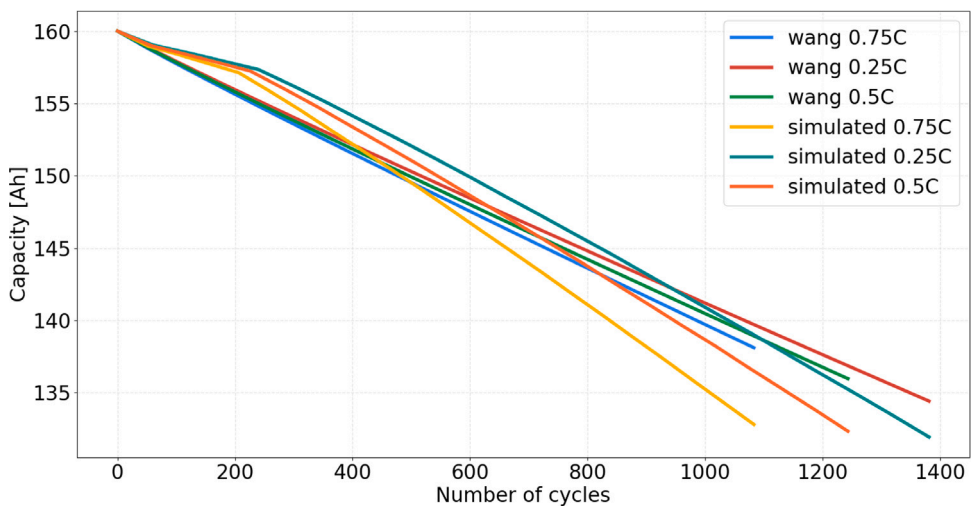

Fig. 9. Wang's model tested at 0.25 C, 0.5 C, and 0.75 C.

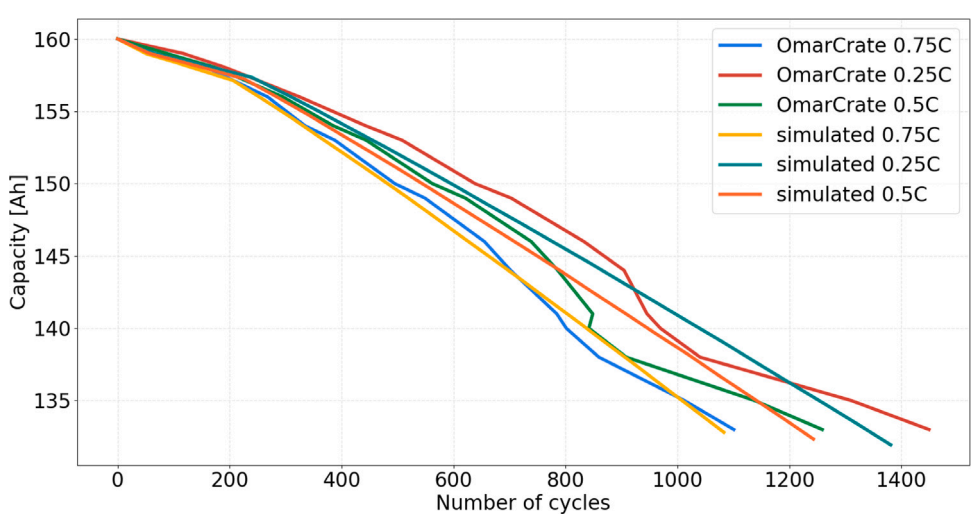

Fig. 10. Omar's model depending on Crate tested at 0.25 C, 0.5 C and 0.75 C.

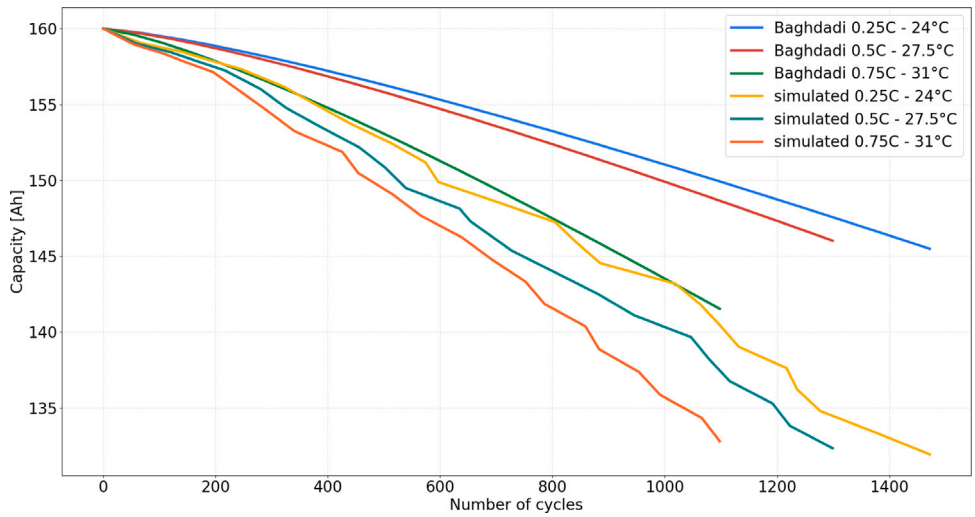

Fig. 11. Baghdadi's model tested at 0.25 C and 24 °C, 0.5 C and 27.5 °C, and 0.75 C and 31 °C.

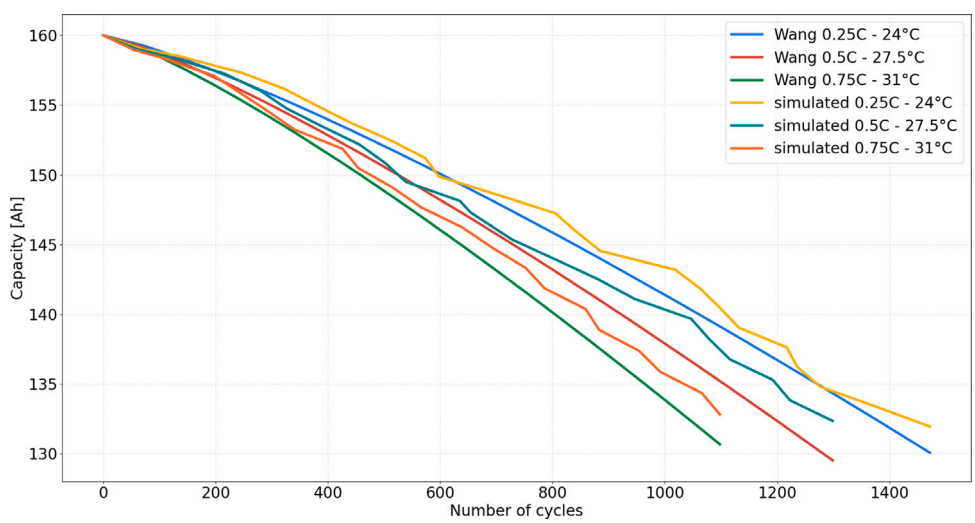

Fig. 12. Wang's model tested at 0.25 C and 24 °C, 0.5 C and 27.5 °C, and 0.75 C and 31 °C.

Table 14
Wang's model parameters related to the multivariate sensitivity analysis.

k1	k2	k3
0.619	1.23	−28754.217

All the models are tested with capacity curves related to pair values of (0.25 C, 24 °C), (0.5 C, 27.5 °C), and (0.75 C, 31 °C). Fig. 11 shows that the Baghdadi's model (red, blue, and green lines) overestimates the simulated data (orange, yellow, and aqua green curves), reaching a maximum error of 14.87 A h, a MAE of 6.15 A h, and a RMSE of 7.54 A h.

Fig. 12 shows that the Wang's model follows the simulated data properly when tested at (0.25 C, 24 °C), (0.5 C, 27.5 °C), and (0.75 C, 31 °C), thus highlighting a great robustness with respect to the variation of both Crate and temperature. The numerical results achieved a maximum error of 3.05 A h, a MAE of 0.96 A h, and a RMSE of 1.25 A h.

The MAPE values computed for the multivariate analysis, which is used to compare the performance of the models, are reported in Table 15: the most robust model related to the temperature and current variation is the Wang's one. It is worth noting that Omar's model has been excluded from this analysis because each of its equations evaluates the aging based only on the variation of a single input quantity; thus, it is not a viable candidate for performing the multivariate analysis. Conversely, the worst performance has been obtained by the Baghdadi's model with a MAE of 14.87 A h compared to 3.05 A h of the Wang' model. Thus, the Wang's model is the most robust and represent the best choice when considering both temperature and current variations simultaneously.

4. Conclusions

This paper presents a sensitivity analysis of battery aging models to evaluate how a model deals with the variation of the storage operating condition on which they have previously been trained. Three aging models proposed in the scientific literature have been included in this

Table 15
MAPE computed for the multivariate sensitivity.

Crate, Temperature	Wang	Baghdadi	Omar
0.25 C, 24 °C	0.55%	4.43%	NA
0.5 C, 27.5 °C	0.76%	4.49%	NA
0.75 C, 31 °C	0.73%	2.79%	NA

study. Simulated data, representing a 160 A h BESS, have been employed to perform both univariate and multivariate analysis to evaluate response to temperature and current variation, which represent the greatest factor impacting the storage SOH.

The results of the sensitivity analysis showed that all the three models were able to predict battery aging under various operating conditions. However, some models were more sensitive to the variation of certain factors than others. Regarding the univariate analysis of temperature, the best model is represented by Baghdadi et al. [32] when dealing with both temperature values of 25 °C and 30 °C. Differently, the model of Wang et al. [27] is the most robust solution when dealing with current variation for values of 0.25 C, 0.5 C and 0.75 C. Furthermore, the multivariate analysis assesses that the model of Wang [27] is the most robust to the simultaneous change of both temperature and current.

Future works could focus on further refining the training of aging models and exploring the impact of other factors on battery degradation. The training on different operating conditions should be included to validate the results obtained by these study, or evaluate the robustness of model to other range of values. These studies may include different values of both temperature and current.

As a potential future development, the training of each battery aging model on different levels of degradation could be an effective way to improve the accuracy of the models. By computing a training phase for smaller range of degradation levels, the models would be able to capture the complexities and nuances of battery aging in a better way, thus leading to more accurate predictions.

Moreover, the inclusion of other mathematical or data-driven models in a future sensitivity analysis of battery aging could provide interesting results. Particularly, data-driven models such as neural networks use deep learning algorithms to identify patterns and non linear relationships in data, and can often provide more accurate predictions than mathematical models, particularly when working with complex systems as batteries.

In conclusion, the sensitivity analysis of the various battery aging models revealed that several factors variation can significantly impact the rate of the battery degradation. These findings suggest which aging model is important to consider according to the design and expected operating conditions of battery storage systems, thus helping to ensure that they are able to meet the demands of the application and maximize their lifespan. By considering all these factors, it may be possible to extend the lifetime of a battery and improve its performance.

CRediT authorship contribution statement

Enrico Marchegiani: Conceptualization, Data curation, Formal analysis, Methodology, Visualization, Writing – original draft, Writing – review & editing. **Francesco Ferracuti:** Conceptualization, Methodology, Visualization, Writing – original draft, Writing – review & editing. **Andrea Monteriù:** Writing – review & editing, Supervision. **Lingkang Jin:** Data curation, Visualization, Writing – original draft, Writing – review & editing. **Mosè Rossi:** Formal analysis, Visualization, Writing – original draft, Writing – review & editing. **Gabriele Comodi:** Supervision, Writing – original draft, Writing – review & editing. **Lucio Ciabattoni:** Conceptualization, Methodology, Supervision, Writing – original draft, Writing – review & editing.

Declaration of competing interest

The authors declare that they have no known competing financial interests or personal relationships that could have appeared to influence the work reported in this paper.

Data availability

Data will be made available on request

References

[1] K. Tan, T. Babu, V.K. Ramachandaramurthy, P. Kasinathan, S. Solanki, S. Raveendran, Empowering smart grid: A comprehensive review of energy storage technology and application with renewable energy integration, J. Energy Storage 39 (2021) 102591, http://dx.doi.org/10.1016/j.est.2021.102591, URL https://www.sciencedirect.com/science/article/pii/S2352152X21003340.

[2] M. Taghikhani, Renewable resources and storage systems stochastic multi-objective optimal energy scheduling considering load and generation uncertainties, J. Energy Storage 43 (2021) 103293, http://dx.doi.org/10.1016/j.est.2021.103293, URL https://www.sciencedirect.com/science/article/pii/S2352152X21009853.

[3] S.A. Bozorgavari, J. Aghaei, S. Pirouzi, V. Vahidinasab, H. Farahmand, M. Korpås, Two-stage hybrid stochastic/robust optimal coordination of distributed battery storage planning and flexible energy management in smart distribution network, J. Energy Storage 26 (2019) 100970, http://dx.doi.org/10.1016/j.est.2019.100970, URL https://www.sciencedirect.com/science/article/pii/S2352152X19306668.

[4] M.D. Rosa, O. Afanaseva, A. Fedyukhin, V. Bianco, Prospects and characteristics of thermal and electrochemical energy storage systems, J. Energy Storage 44 (Part B) (2021) 103443, http://dx.doi.org/10.1016/j.est.2021.103443, URL https://www.sciencedirect.com/science/article/pii/S2352152X21011257.

[5] C. Das, T. Mahmoud, O. Bass, S. Muyeen, G. Kothapalli, A. Baniasadi, N. Mousavi, Optimal sizing of a utility-scale energy storage system in transmission networks to improve frequency response, J. Energy Storage 29 (2020) 101315, http://dx.doi.org/10.1016/j.est.2020.101315, URL https://www.sciencedirect.com/science/article/pii/S2352152X19315646.

[6] A. Ramos, M. Tuovinen, M. Ala-Juusela, Battery energy storage system (BESS) as a service in Finland: Business model and regulatory challenges, J. Energy Storage 40 (2021) 102720, http://dx.doi.org/10.1016/j.est.2021.102720, URL https://www.sciencedirect.com/science/article/pii/S2352152X21004552?via%3Dihub.

[7] W.W. Abdullah, M. Osman, M.A.A. Kadir, R. Verayiah, N.A. Aziz, M.A. Rasheed, Techno-economics analysis of battery energy storage system (BESS) design for virtual power plant (VPP)–A case study in Malaysia, J. Energy Storage 38 (2021) 102568, http://dx.doi.org/10.1016/j.est.2021.102568, URL https://www.sciencedirect.com/science/article/pii/S2352152X21003133?via%3Dihub.

[8] P. Saini, L. Gidwani, An investigation for battery energy storage system installation with renewable energy resources in distribution system by considering residential, commercial and industrial load models, J. Energy Storage 45 (2022) 103493, http://dx.doi.org/10.1016/j.est.2021.103493, URL https://www.sciencedirect.com/science/article/pii/S2352152X21011762?via%3Dihub.

[9] M. Mustafa, P. Keatley, Y. Huang, O. Agbonaye, O. Ademulegun, N. Hewitt, Evaluation of a battery energy storage system in hospitals for arbitrage and ancillary services, J. Energy Storage 43 (2021) 103183, http://dx.doi.org/10.1016/j.est.2021.103183, URL https://www.sciencedirect.com/science/article/pii/S2352152X21008835?via%3Dihub.

[10] A. Bartolini, F. Carducci, C.B. Muñoz, G. Comodi, Energy storage and multi energy systems in local energy communities with high renewable energy penetration, Renew. Energy 159 (2020) 595–609, http://dx.doi.org/10.1016/j.renene.2020.05.131, URL https://www.sciencedirect.com/science/article/pii/S0960148120308351.

[11] M. Jafari, K. Khan, L. Gauchia, Deterministic models of li-ion battery aging: It is a matter of scale, J. Energy Storage 20 (2018) 67–77, http://dx.doi.org/10.1016/j.est.2018.09.002, URL https://www.sciencedirect.com/science/article/pii/S2352152X18303098?via%3Dihub.

[12] M. Casals, B. Garcia, F. Aguesse, A. Iturrondobeitia, Second life of electric vehicle batteries: relation between materials degradation and environmental impact, Int. J. Life Cycle Assess. 22 (2017) 82–97, http://dx.doi.org/10.1007/s11367-015-0918-3.

[13] S. Atalay, M. Sheikh, A. Mariani, Y. Merla, E. Bower, W.D. Widanage, Theory of battery ageing in a lithium-ion battery: Capacity fade, nonlinear ageing and lifetime prediction, J. Power Sources 478 (2020) 229026, http://dx.doi.org/10.1016/j.jpowsour.2020.229026, URL https://www.sciencedirect.com/science/article/pii/S0378775320313239?via%3Dihub.

[14] M. Ecker, N. Nieto, S. Käbitz, J. Schmalstieg, H. Blanke, A. Warnecke, D. UweSauer, Calendar and cycle life study of Li(NiMnCo)O2-based 18650 lithium-ion batteries, J. Power Sources 248 (2014) 839–851, http://dx.doi.org/10.1016/j.jpowsour.2013.09.143, URL https://www.sciencedirect.com/science/article/pii/S0378775313016510.

[15] S.F. Schuster, T. Bach, E. Fleder, J. Müller, M. Brand, G. Sextl, A. Jossen, Nonlinear aging characteristics of lithium-ion cells under different operational conditions, J. Energy Storage 1 (2015) 44–53, http://dx.doi.org/10.1016/j.est.2015.05.003, URL https://www.sciencedirect.com/science/article/pii/S2352152X15000092.

[16] G. Rancilio, A. Lucas, E. Kotsakis, G. Fulli, M. Merlo, M. Delfanti, M. Masera, Modeling a large-scale battery energy storage system for power grid application analysis, Energies 12 (17) (2019) http://dx.doi.org/10.3390/en12173312.

[17] O. Tremblay, L.-A. Dessaint, Experimental validation of a battery dynamic model for EV applications, World Electr. Veh. J. 3 (2) (2009) 289–298, http://dx.doi.org/10.3390/wevj3020289.

[18] T. Huria, M. Ceraolo, J. Gazzarri, R. Jackey, High fidelity electrical model with thermal dependence for characterization and simulation of high power lithium battery cells, in: 2012 IEEE International Electric Vehicle Conference, 2012, pp. 1–8, http://dx.doi.org/10.1109/IEVC.2012.6183271.

[19] J.V. Barreras, E. Schaltz, S.J. Andreasen, T. Minko, Datasheet-based modeling of li-ion batteries, in: 2012 IEEE Vehicle Power and Propulsion Conference, 2012, pp. 830–835, http://dx.doi.org/10.1109/VPPC.2012.6422730.

[20] C. Guenther, B. Schott, W. Hennings, P. Waldowski, M.A. Danzer, Model-based investigation of electric vehicle battery aging by means of vehicle-to-grid scenario simulations, J. Power Sources 239 (2013) 604–610, http://dx.doi.org/10.1016/j.jpowsour.2013.02.041, URL https://www.sciencedirect.com/science/article/pii/S0378775313003066.

[21] S.J. Moura, N.A. Chaturvedi, M. Krstić, Adaptive partial differential equation observer for battery state-of-charge/state-of-health estimation via an electrochemical model, J. Dyn. Syst. Meas. Control 136 (1) (2013) http://dx.doi.org/10.1115/1.4024801, 011015. arXiv:https://asmedigitalcollection.asme.org/dynamicsystems/article-pdf/136/1/011015/6115560/ds_136_01_011015.pdf.

[22] N. Omar, Y. Firouz, H. Gualous, J. Salminen, T. Kallio, J. Timmermans, T. Coosemans, P. Van den Bossche, J. Van Mierlo, 9 - aging and degradation of lithium-ion batteries, in: A.A. Franco (Ed.), Rechargeable Lithium Batteries, in: Woodhead Publishing Series in Energy, Woodhead Publishing, 2015, pp. 263–279, http://dx.doi.org/10.1016/B978-1-78242-090-3.00009-2, URL https://www.sciencedirect.com/science/article/pii/B9781782420903000092.

[23] A. Farmann, W. Waag, A. Marongiu, D.U. Sauer, Critical review of on-board capacity estimation techniques for lithium-ion batteries in electric and hybrid electric vehicles, J. Power Sources 281 (2015) 114–130, http://dx.doi.org/10.1016/j.jpowsour.2015.01.129, URL https://www.sciencedirect.com/science/article/pii/S0378775315001457.

[24] M. Berecibar, I. Gandiaga, I. Villarreal, N. Omar, J. Van Mierlo, P. Van den Bossche, Critical review of state of health estimation methods of li-ion batteries for real applications, Renew. Sustain. Energy Rev. 56 (2016) 572–587, http://dx.doi.org/10.1016/j.rser.2015.11.042, URL https://www.sciencedirect.com/science/article/pii/S1364032115013076.

[25] S. Barcellona, L. Piegari, Lithium ion battery models and parameter identification techniques, Energies 10 (12) (2017) http://dx.doi.org/10.3390/en10122007, URL https://www.mdpi.com/1996-1073/10/12/2007.

[26] D.-I. Stroe, M. Swierczynski, S.K. Kær, R. Teodorescu, Degradation behavior of lithium-ion batteries during calendar ageing—The case of the internal resistance increase, IEEE Trans. Ind. Appl. 54 (1) (2018) 517–525, http://dx.doi.org/10.1109/TIA.2017.2756026.

[27] J. Wang, P. Liu, J. Hicks-Garner, E. Sherman, S. Soukiazian, M. Verbrugge, H. Tataria, J. Musser, P. Finamore, Cycle-life model for graphite-LiFePO4 cells, J. Power Sources 196 (8) (2011) 3942–3948, http://dx.doi.org/10.1016/j.jpowsour.2010.11.134, URL https://www.sciencedirect.com/science/article/pii/S0378775310021269.

[28] T. Yuksel, S. Litster, V. Viswanathan, J.J. Michalek, Plug-in hybrid electric vehicle LiFePO4 battery life implications of thermal management, driving conditions, and regional climate, J. Power Sources 338 (2017) 49–64, http://dx.doi.org/10.1016/j.jpowsour.2016.10.104, URL https://www.sciencedirect.com/science/article/pii/S0378775316315130.

[29] S. Li, H. He, C. Su, P. Zhao, Data driven battery modeling and management method with aging phenomenon considered, Appl. Energy 275 (2020) 115340, http://dx.doi.org/10.1016/j.apenergy.2020.115340, URL https://www.sciencedirect.com/science/article/pii/S0306261920308527.

[30] N. Omar, M.A. Monem, Y. Firouz, J. Salminen, J. Smekens, O. Hegazy, H. Gaulous, G. Mulder, P. Van den Bossche, T. Coosemans, J. Van Mierlo, Lithium iron phosphate based battery – Assessment of the aging parameters and development of cycle life model, Appl. Energy 113 (2014) 1575–1585, http://dx.doi.org/10.1016/j.apenergy.2013.09.003, URL https://www.sciencedirect.com/science/article/pii/S0306261913007393.

[31] E. Sarasketa-Zabala, E. Martinez-Laserna, M. Berecibar, I. Gandiaga, L. Rodriguez-Martinez, I. Villarreal, Realistic lifetime prediction approach for Li-ion batteries, Appl. Energy 162 (2016) 839–852, http://dx.doi.org/10.1016/j.apenergy.2015.10.115, URL https://www.sciencedirect.com/science/article/pii/S0306261915013513.

[32] I. Baghdadi, O. Briat, J.-Y. Delétage, P. Gyan, J.-M. Vinassa, Lithium battery aging model based on Dakin's degradation approach, J. Power Sources 325 (2016) 273–285, http://dx.doi.org/10.1016/j.jpowsour.2016.06.036, URL https://www.sciencedirect.com/science/article/pii/S0378775316307388.

[33] M.F. Ng, J. Zhao, Q. Yan, G.J. Conduit, Z.W. Seh, Predicting the state of charge and health of batteries using data-driven machine learning, Nat. Mach. Intell. 2 (2020) 161–170, http://dx.doi.org/10.1038/s42256-020-0156-7.

[34] H. Huang, J. Meng, Y. Wang, L. Cai, J. Peng, J. Wu, Q. Xiao, T. Liu, R. Teodorescu, An enhanced data-driven model for lithium-ion battery state-of-health estimation with optimized features and prior knowledge, Automot. Innov. 5 (2022) 134–145, http://dx.doi.org/10.1007/s42154-022-00175-3.

[35] C. Birkl, Oxford Battery Degradation Dataset 1, University of Oxford, 2017, http://dx.doi.org/10.5287/BODLEIAN:KO2KDMYGG.

[36] Battery Data | Center for Advanced Life Cycle Engineering. URL https://calce.umd.edu/battery-data,

[37] N. Harting, R. Schenkendorf, N. Wolff, U. Krewer, State-of-health identification of lithium-ion batteries based on nonlinear frequency response analysis: First steps with machine learning, Appl. Sci. 8 (5) (2018) http://dx.doi.org/10.3390/app8050821, URL https://www.mdpi.com/2076-3417/8/5/821.

[38] H. Pan, Z. Lü, H. Wang, H. Wei, L. Chen, Novel battery state-of-health online estimation method using multiple health indicators and an extreme learning machine, Energy 160 (2018) 466–477, http://dx.doi.org/10.1016/j.energy.2018.06.220, URL https://www.sciencedirect.com/science/article/pii/S0360544218312854.

[39] L. Fang, J. Li, B. Peng, Online estimation and error analysis of both SOC and SOH of lithium-ion battery based on DEKF method, Energy Procedia 158 (2019) 3008–3013, http://dx.doi.org/10.1016/j.egypro.2019.01.974, Innovative Solutions for Energy Transitions. URL https://www.sciencedirect.com/science/article/pii/S1876610219310264.

[40] D. Andre, C. Appel, T. Soczka-Guth, D.U. Sauer, Advanced mathematical methods of SOC and SOH estimation for lithium-ion batteries, J. Power Sources 224 (2013) 20–27.

[41] S. Khaleghi, Y. Firouz, M. Berecibar, J.V. Mierlo, P.V.D. Bossche, Ensemble gradient boosted tree for SoH estimation based on diagnostic features, Energies 13 (5) (2020) http://dx.doi.org/10.3390/en13051262, URL https://www.mdpi.com/1996-1073/13/5/1262.

[42] J. Meng, L. Cai, D.-I. Stroe, J. Ma, G. Luo, R. Teodorescu, An optimized ensemble learning framework for lithium-ion battery state of health estimation in energy storage system, Energy 206 (2020) 118140, http://dx.doi.org/10.1016/j.energy.2020.118140, URL https://www.sciencedirect.com/science/article/pii/S0360544220312470.

[43] S. Song, C. Fei, H. Xia, Lithium-ion battery SOH estimation based on XGBoost algorithm with accuracy correction, Energies 13 (4) (2020) http://dx.doi.org/10.3390/en13040812, URL https://www.mdpi.com/1996-1073/13/4/812.

[44] C. Vidal, P. Malysz, P. Kollmeyer, A. Emadi, Machine learning applied to electrified vehicle battery state of charge and state of health estimation: State-of-the-art, IEEE Access 8 (2020) 52796–52814, http://dx.doi.org/10.1109/ACCESS.2020.2980961.

[45] M. Ragone, V. Yurkiv, A. Ramasubramanian, B. Kashir, F. Mashayek, Data driven estimation of electric vehicle battery state-of-charge informed by automotive simulations and multi-physics modeling, J. Power Sources 483 (2021) 229108, http://dx.doi.org/10.1016/j.jpowsour.2020.229108, URL https://www.sciencedirect.com/science/article/pii/S0378775320314038.

[46] S. Yang, C. Zhang, J. Jiang, W. Zhang, L. Zhang, Y. Wang, Review on state-of-health of lithium-ion batteries: Characterizations, estimations and applications, J. Clean. Prod. 314 (2021) http://dx.doi.org/10.1016/j.jclepro.2021.128015.

[47] H. Tian, P. Qin, K. Li, Z. Zhao, A review of the state of health for lithium-ion batteries: Research status and suggestions, 2020, http://dx.doi.org/10.1016/j.jclepro.2020.120813, URL https://doi.org/10.1016/j.jclepro.2020.120813.

[48] M. Broussely, P. Biensan, F. Bonhomme, P. Blanchard, S. Herreyre, K. Nechev, R. Staniewicz, Main aging mechanisms in Li ion batteries, J. Power Sources 146 (1–2) (2005) 90–96.

[49] A. Łebkowski, Temperature, overcharge and short-circuit studies of batteries used in electric vehicles, Prz. Elektrotech. 1 (5) (2017) 69–75.

[50] Y. Bao, W. Dong, D. Wang, Online internal resistance measurement application in lithium ion battery capacity and state of charge estimation, Energies 11 (5) (2018) 1073.

[51] S. Ma, M. Jiang, P. Tao, C. Song, J. Wu, J. Wang, T. Deng, W. Shang, Temperature effect and thermal impact in lithium-ion batteries: A review, Prog. Nat. Sci. Mater. Int. 28 (6) (2018) 653–666.

[52] J. Guo, Y. Li, K. Pedersen, D.-I. Stroe, Lithium-ion battery operation, degradation, and aging mechanism in electric vehicles: An overview, Energies 14 (17) (2021) 5220.

[53] R. Poli, J. Kennedy, T. Blackwell, Particle swarm optimization, Swarm Intell. 1 (1) (2007) 33–57.

[54] N. Gebraeel, Sensory-updated residual life distributions for components with exponential degradation patterns, IEEE Trans. Autom. Sci. Eng. 3 (4) (2006) 382–393.